Biochimica et Biophysica Acta, 1061 (1991) 65–77

0005-2736/91/$03.50
ADONIS 000527369100054Z

BBAMEM 75082

A microscopic electrostatic model for the amphotericin B channel

Marcial Bonilla-Marín [1], Matilde Moreno-Bello [1] and Iván Ortega-Blake [2]

[1] *Laboratorio de Biofísica, Depto. de Física, Facultad de Ciencias, Universidad Nacional Autónoma de México, Mexico City (Mexico)* and [2] *Laboratorio de Cuernavaca, Instituto de Física, Universidad Nacional Autónoma de México, Cuernavaca, Morelos (Mexico)*

(Received 18 December 1989)
(Revised manuscript received 21 May 1990)

Key words: Antibiotic; Polyene; Selectivity; Permeability; Channel; Ionophore

A microscopic model of an amphotericin B channel is proposed. The structure of the pores is generated using the atomic coordinates of the molecule in the structure determined experimentally by X-ray diffraction. The net charges of the atoms are determined by Mulliken analysis. With these charges the electrostatic energy profiles are calculated for a monovalent ion passing through the channels formed by different number of antibiotic molecules having different radii. The water inside the channel was considered through a continuum medium using the dielectric constant of the bulk, and the membrane contribution was included using the virtual images of the pore in a dielectric slab of $\varepsilon = 3$. The model satisfactorily explains the permeability and selectivity characteristics as well as other observations yet unexplained. The electrostatic profiles obtained reinforce the hypothesis of the existence of channels formed by a variable number of units.

Introduction

One of the most common mechanisms for ion transport through membranes is the diffusion through hydrated channels, which are formed by very specific molecules. The understanding of the formation of these channels and how their selectivities are attained is, to some extent, an open question. In membranes treated by external agents such as antibiotics, drugs, detergents, etc., there are observations which have permitted models for the formation of channels [1,2] to be put forward. For polyene antibiotics, such as amphotericin B, there is substantial phenomenological information that has permitted a structural model to be developed since the early 1970's [3–7].

These antibiotics are of great importance because of their specific activity against fungi and yeast and, therefore, they are used against mycotic infections. In particular amphotericin B, besides its importance in medicine, has the advantage of being accessible in a high degree of purity and since the crystallization of the biologically active *N*-iodoacetylamphotericin-B by Ganis et al. [8], its molecular structure is known. Roughly, the molecule presents a closed rectangular configuration formed by a heptane chromophore and a saturated carbon chain. The polar head consists of two chairs: a mycosamine ring and a ketal ring; at the tail some methyl groups are found. The actual structure of the molecule is presented in Fig. 1. The coordinates of the heavy atoms as presented in Ref. 8 and those of the hydrogen atoms used in the present work are given in Table II.

Keeping this structure in mind, it is easy to see that the aggregation of monomers in clusters inside the membrane responds to the interactions between themselves and the hydrophobic media. For the formation of amphotericin B channels the presence of sterols is required and one can, therefore, advance the idea that the hydrophobic side of the antibiotic will interact with the membrane lipids and the sterols to leave the hydrophilic part, rejected by the lipidic membrane to form the hydrated pore. This will conduce to the hydrophilic channel shown in Fig. 2 proposed by Andreoli [7] and De Kruijff and Demel [3]. The sterol-antibiotic stoichiometries reported vary from 0.7 to 3.9 [3], which suggest that it is possible to have channels formed by different number of monomeric units. In fact, several pore sizes have been reported [3,4,5,9], with the number of monomers per pore ranging from 4 to 12. It is quite surprising to have such a spectrum of molecular confor-

Abbreviations: SLC, single length channel; DLC, double length channel.

Correspondence: M. Bonilla-Marín, Laboratorio de Biofísica, Depto. de Física, Facultad de Ciencias, Universidad Nacional Autónoma de México, Apdo. Postal 21-939, C.P. 04000 Mexico City, Mexico.

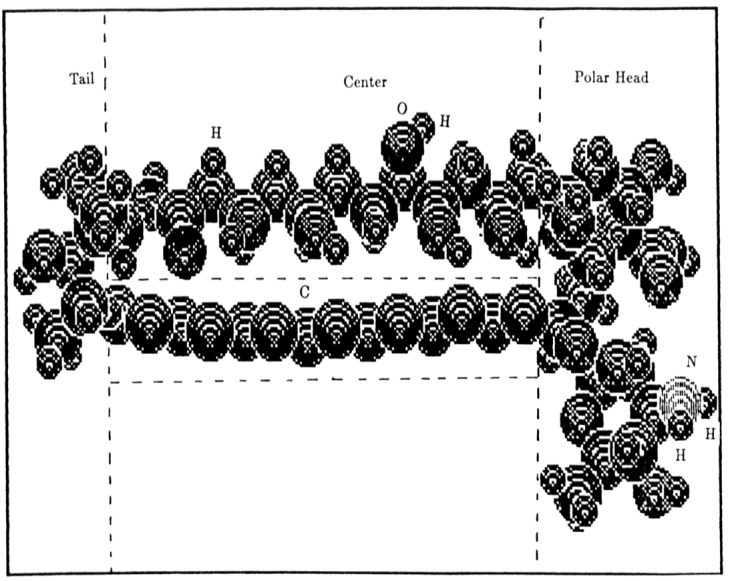

Fig. 1. Structure of the amphotericin B molecule from the crystallographic data of Ganis et al. [8]. For computational purposes the molecule was partitioned in the three fragments indicated. The central fragment did not consider the chromophore heptane that does not face the hydrated interior as it is considered part of the membrane.

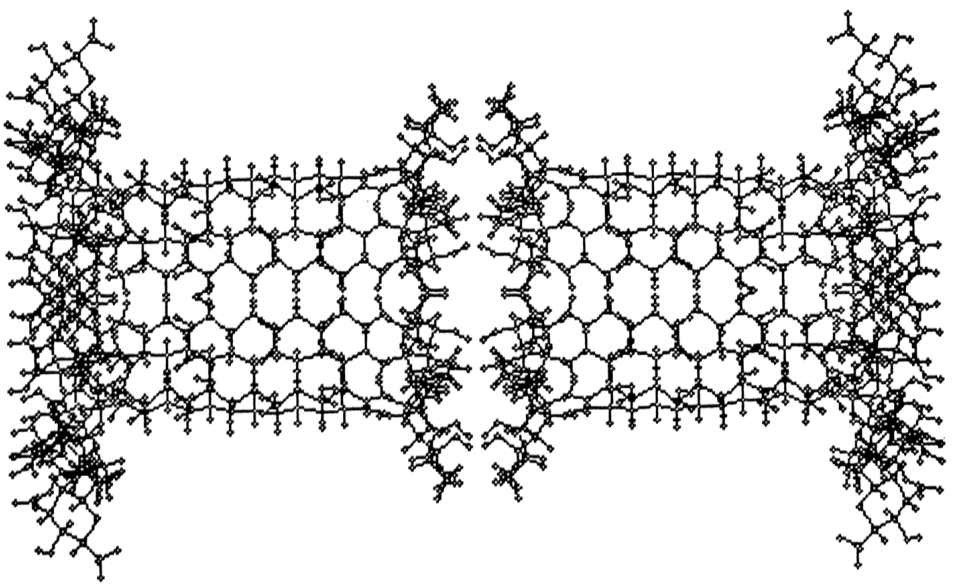

Fig. 2. The structure of the double-length channel of amphotericin B. The figure was constructed by simple reflexion of a single-length channel through the plane perpendicular to the channel axis and passing through the tails. As a consequence of this there are many atom-atom close approaches; in reality the double-length pore will be formed by turning one pore over the other.

mations. Furthermore, in spite of this variability, the selectivity does not seem to change.

When the antibiotic is added to only one side of the membrane a single-length channel (SLC) is formed, whereas for a thicker membrane, greater than 24.0 ± 0.5 Å [6], it is necessary to add the antibiotic to both sides of the membrane in order to obtain a double-length channel (DLC), as shown in Fig. 2; the SLC corresponds to half the figure. SLC are selective to monovalent cations while DLC are selective to monovalent anions [6].

Selectivity and permeability to ions in channels has been described in terms of electrostatic potentials since Parsegian (1969) [10] for channels with uniform density and infinite length. Later on, Levitt (1978) [11,12] studied the same problem for finite length and obtained the energy barriers for one, two and three ions in the gramicidin channel. Jordan [13,14] and Sung and Jordan [15], study some electrostatic aspects of the membrane and the pore, taking into account the effects produced by the surface density charge. There are of course simplifications needed to attack such an enormous computational task. They are mainly the neglect in the model of all the parts of the molecule which do not face directly the hydrated interior. Also, water is only included in a bulk manner, not accounting for the structural interaction. Certainly the numerical values will not be exact, but it is believed that the picture is qualitatively reliable.

In this work, we put forward a microscopic model for both amphotericin B channels, SLC and DLC. We look into the structure of these channels for different pore radii and number of monomeric units. With the proposed structures we look into the profiles of the electrostatic potential energy along the channel axis, obtained from a net charge description of the monomer given by quantum mechanical calculations of a restricted monomeric unit. The water effect is incorporated in these profiles through the assumption of a continuum dielectric constant $\varepsilon = 80$, and the contribution of the membrane to the electric field is accounted for by considering the images of the pore net charges in a continuum dielectric slab ($\varepsilon = 3$) with the membrane dimensions. In terms of these profiles we advance an explanation for the selectivity behaviour observed. Furthermore, the microscopic character of the model permits the identification of regions in the molecule strongly involved in the formation of the pore complex, in the selectivity to anions or in the selectivity to cations. Finally, we use the proposed model to explain several experimental observations.

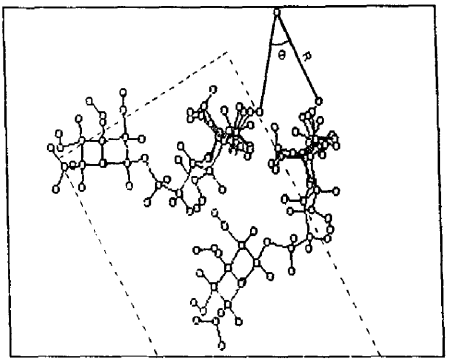

Fig. 3. Top side view of the pore. Here we present a dimer which characterizes a channel constructed with a radius of 4.47 Å and an angle between units $\theta = 45°$. We are indicating the region of closest approach.

Methods

Pore construction

A restricted monomer, consisting of the amphotericin B molecule minus the heptane chromophore that does not face the hydrated interior, is placed at a radius R from an axis parallel to the molecule chains. This unit is rotated n times an angle $2\pi/n$ around this axis yielding a closed n-mer. The dimer, which characterizes a pore, is presented in Fig. 3. The radius of the pore is determined by constructing a channel in which there is no

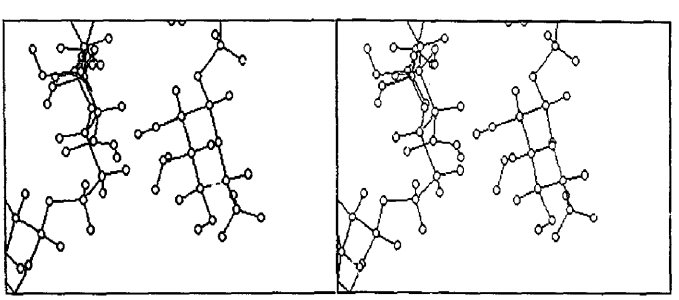

Fig. 4. Stereo par of the region indicated in Fig. 3 where a close encounter between keto and amino chairs of two neighboring molecules occurs. Notice that there is substantial room for hydrogen bonding if one allows for rotation of H's and NH's.

overlap of the Van der Waals radii of the atoms. Inspection of Fig. 3 shows that there is a particular region where a close encounter between the ketal and the mycosamine chairs of two neighboring units occurs (see Fig. 4). However, close examination of this region shows that several intermolecular hydrogen bonds can be formed. Of course, for the pore stability, the interaction of the molecule with the lipid, water and sterols should be considered, but given the local character of these hydrogen bonds, one can expect it to play an important role in the formation of the pore, giving stability to the structure.

As a result of the proposed structure one can identify three regions forming the pore: (i) The mouth which is constituted by the ketal and amino chairs, which looks like a crater with the amino chair in the more external region and in the internal slope the ketal chair. (ii) The central part of the pore, i.e., the hydrophilic interior of almost constant radius, formed by the saturated chain of the macro-ring. (iii) The tail constituted by the end of the chains which presents some methyl groups. These fragments are indicated in Fig. 1.

For DLC the three regions previously described are present twice, leaving a symmetric structure respect to the center of the channel. In this case both terminal parts of the pore are mouths, as described before, while the union of the tails of the single monomers become the new central region (Fig. 2).

Model construction

Once we have the molecular structure of the pore, we can attempt to understand the passage of ions which will be produced by transmembranal electric potential difference. This pasage will be affected not only by steric factors, but also by the electrostatic potential energy profiles that ions feel through the channel. Normally ad-hoc assumptions are made to permit the advance of such electrostatic profiles which in turn should show agreement with experiment. An alternative way is to obtain the image potential through calculated microscopic properties. Obviously, in a complex of such dimensions an accurate complete treatment is not possible, hence several, well-defined approximations ought to be made to obtain this potential.

In this work, we construct the electrostatic potential energy through the description of atomic net charges in the molecule obtained from ab-initio molecular orbital calculations. These calculations were done using the HF-SCF method with the LCAO Scheme. The ab-initio pseudopotentials of Barthelat et al. [16] were used with the HONDO program of King et al. [17]. A minimal basis set consisting of four gaussian primitives contracted to one function was used. This molecular approach is now well established, and in spite of being the more economical basis set, in computational terms, it is well suited for obtaining the electronic structure of the molecule (see for example Ref. 18).

In order to make the molecular orbital calculations we proceeded as follows:

(i) The molecule was restricted to the atoms facing the hydrophilic pore, the chromophore heptane chain and the contributions that arise from sterols and lipids are considered, forming part of a surrounding dielectric slab with $\varepsilon = 3$ with the membrane dimensions.

(ii) The molecular calculations were performed in three fragments of approx. 40–50 atoms each, keeping intact chemical groups and saturating the free bonds with hydrogen atoms. The actual partition scheme is indicated in Fig. 1.

(iii) The whole molecule net charges were reconstituted using the net charges computed through Mulliken analysis of the three fragments. Hence, intramolecular non-additivity that could modify the electronic distribution was not considered, neither intermolecular non-additivity when the monomeric unit was used to obtain the pore electrostatic profile or the electrostatic interaction energy.

It is known that the pore selectivity is independent of the membrane sterols and surface charge [6]; this is a clear indication that the most relevant processes of ionic selectivity for these types of channel are due to the pore itself and, therefore, the neglect of the environment of the pore (sterols, membrane charge, lipids) can be an adequate approximation. This is also supported by the fact that for a single length pore the length of the molecule is larger than the width of the membrane, showing that the pore is protruding to a large extent. The relative permeabilities to nonelectrolytes [6]

$$(P_{\text{urea}}/P_{\text{glycerol}})_{\text{single}} \simeq (P_{\text{urea}}/P_{\text{glycerol}})_{\text{double}}$$

supports the idea that single and double length pores have the same structure and it is in agreement with the assumption of having SLC joined by hydrogen bonds to produce DLC. Our model also considers that a DLC is just twice a SLC.

A critical approximation of our model is to assume that the intermolecular potential is given by the classical electrostatic interaction. We think this approximation is sound because of the large dipole moment of the antibiotic; the expected values of the dipole moments for the three fragments are presented in Table I, which indicate a large value for the whole molecule. With such a large dipole, the intermolecular forces at distances larger than 4 Å will be determined mainly by the electrostatic contributions.

The lack of microscopic detail present in the assumption of bulk water inside the pore can be adequate only for broad channels, where water dipoles can orient and screen the net charges, as is the case of amphotericin

TABLE I

Dipolar moment components (in debyes) obtained as the expectation value of the dipole moment in the molecular orbital calculations of the three fragments of the amphotericin B molecule of Fig. 1

When a pore is formed, by axial symmetry, the X and Y components cancel at the Z axis and only the electric field will be due only to the superposition of the Z components. The pore is placed with its mouth at $Z = 0$ and the tail pointing in the negative Z direction for this calculation.

Segment	$\|P\|$	P_x	P_y	P_z
Head	7.25	6.81	0.59	2.49
Center	9.83	6.23	−0.76	7.57
Tail	1.95	0.07	1.49	−1.25

with a radius of approx. 5 Å compared to gramicidin with $R \approx 2$ Å. Nonetheless, even for the channels considered here, water will be structured and it is difficult to guess effects that this will produce. From the molecular dynamics simulation of water in pores (see for example Ref. 19) the ion seems to produce a single file of water with considerable amount of orientational freedom. These results were obtained for narrow channels, in amphotericin B one could expect that the whole first hydration shell of the ion could be accommodated (see for example Ref. 20), and if there is the same orientation freedom the bulk phase model would be a good approximation. There is, however, a strong drawback in the simulation presented until now, the lack of non-additivity in the intermolecular interaction, i.e., the ion will produce a strong change in the electronic distribution of the channel and the waters interacting with it [20]. This would conduce to a more structured picture of the phenomena. For instance, inclusion of non-additive effects in liquid water simulations have produced more pronounced structure [21]. It is clear that our model can be refined to account for more microscopic detail and better approximation of the molecular interactions involved. These refinements on the one hand will test the model for convergence of its predictions and shed light on the more general aspect of molecular structure for passage of ions. The validity of the present results rest on the fact that none of them is expected to be strongly modified upon refinement, and most important the very good agreement shown with the experimental evidence so far reported.

The electric gradient that the passing ion feels comes from the atomic net charges that the channel presents to the solution, but there is also a contribution coming from the membrane surrounding the pore. One can take this into account in an approximate way, considering the images of each monomer reflected in the membrane [22]. Fig. 5 shows that there are actually two reflections, one on the side of the membrane holding the monomer considered and another on the opposite side. Note that here we have considered the pore mouth reflected parallel to the membrane, whereas center and tail are reflected perpendicularly, as suggested from the molecular structure. We consider that the net charges used to construct the electric field are in solution, thus reflected in the membrane, instead of considering inside the membrane. The reason for this is that refinement of the model can proceed by substituting the bulk assumption for water molecules interacting with the antibiotic external face, that will be also reflected in the membrane.

Following Andreoli [7] and De Kruijff and Demel [3], one can construct a pore. Here we used the crystallographic coordinates of the molecule given by Ganis et al. [8], and taking care of not to overlap the Van der Waals radii of the atoms, proceeded to build possible pore structures. In addition, we used the Mulliken net charges to obtain an electrostatic intermolecular potential between monomers that serves as a guidance in the construction of the pore. Computer manipulation can then yield reasonable structures. As it was noted before, particular attention has to be given to the hydrogen bonded region which seems to be locking the monomers.

The above procedure produced geometrical structures for the complete pores and the electrostatic potential within them. Because of the assumption of additivity, the electrostatic potential energy obtained for pores with different number of units, has the same form but different numerical values due to the different molecularity that they present, see Fig. 11. Also the DLC electrostatic potential energy is the result of the superposition of two SLC tail-to-tail potentials, see Fig. 7.

We would like to point out that with the above considerations the intrinsic electrostatic potential energy values within the pore are of the order of 1 to 2 kT units, a value much closer to those required for pore

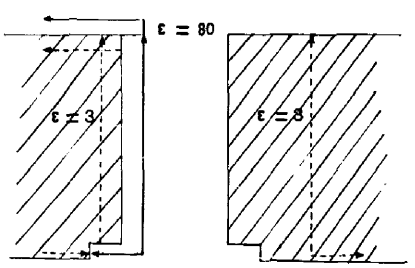

Fig. 5. Schematic representation of a channel at the interface of two dielectric media with $\varepsilon = 3$ for the membrane and $\varepsilon = 80$ for water. The figure illustrates the reflections considered in the image method used in the calculation of the electrostatic profiles, according to Ref. 22. Two reflections are shown, one on the side of the membrane holding the monomer and another on the opposite side. The pore mouth was reflected paralliel to the membrane, whereas center and tail were perpendicular, as suggested from the molecular structure.

TABLE II

Coordinates and charges of the atoms of the amphotericin B molecule used to generate the electrostatic profiles

The charges were obtained by molecular orbital calculations (see text), and the coordinates are those of Ganis et al. [8].

X	*Y*	*Z*	Charge	Atom	*X*	*Y*	*Z*	Charge	Atom
−2.035	5.973	5.145	0.17059	C-13	−1.034	6.231	14.039	−0.40982	C-6
−3.101	5.103	5.024	−0.54234	O-13	−1.959	6.325	12.713	−0.40215	C-7
−2.390	7.317	5.219	−0.41390	O-13	−1.090	5.931	11.509	−0.00729	C-8
−1.078	5.770	3.942	−0.42766	C-14	−0.546	4.656	11.577	−0.53660	O-8
−1.684	6.302	2.606	−0.01802	C-15	−2.017	6.137	10.227	−0.02361	C-9
−0.688	6.277	1.618	−0.53814	O-15	−3.212	5.373	10.385	−0.54689	O-9
−2.146	7.746	2.867	−0.23125	C-16	−1.220	5.682	8.967	−0.41682	C-10
−3.111	7.749	4.048	−0.00942	C-17	−2.026	6.202	7.739	−0.03136	C-11
−3.594	9.231	4.327	−0.41684	C-18	−3.186	5.472	7.676	−0.54829	O-11
−4.793	9.143	5.303	−0.23574	C-19	−1.295	5.694	6.475	−0.63233	C-12
−2.889	8.342	1.581	0.51666	C-41	−3.280	5.113	18.625	0.35452	HO-3
−3.964	7.790	1.352	−0.46380	O-41	−3.557	5.535	14.382	0.33317	HO-5
−2.296	9.131	0.883	−0.57616	O-41P	−0.000	4.472	10.770	0.33775	HO-8
−5.835	8.188	4.865	−0.40544	O-19	−3.801	5.490	9.596	0.36064	HO-9
−6.792	8.720	4.024	0.16301	C-42	−3.736	5.768	6.906	0.33598	HO-11
−7.994	9.014	4.821	−0.39973	O-42	−2.812	5.634	12.791	0.22401	HC-7
−7.137	7.619	2.956	−0.01617	C-43	−2.331	7.351	12.576	0.20552	HC-7
−7.521	6.396	3.644	−0.52777	O-43	−0.293	7.044	14.076	0.26026	HC-6
−8.356	0.085	2.113	−0.15128	C-44	−0.516	5.261	14.057	0.23268	HC-6
−9.471	8.379	2.942	−0.05136	C-45	−0.687	5.186	16.456	0.72995	HC-4
−10.552	9.001	2.185	−0.53123	O-45	−0.326	6.946	16.458	0.19731	HC-4
−9.200	9.438	4.006	−0.03131	C-46	−0.355	7.124	19.111	0.22312	HC-2
−10.167	9.776	5.058	−0.63136	C-47	−0.450	5.332	19.037	0.24928	HC-2
−8.577	6.942	1.174	−0.61790	N	−1.145	4.584	8.957	0.22816	HC-10
−7.743	6.688	2.987	0.34585	HO-43	−0.211	6.118	8.993	0.20500	HC-10
−10.836	8.408	1.443	0.31956	HO-45	−2.564	7.273	17.800	0.21503	HC-3
−9.718	9.585	6.043	0.24448	HC-47	−2.456	7.372	15.239	0.19324	HC-5
−10.440	10.838	4.978	0.21554	HC-47	−0.247	6.632	11.422	0.19226	HC-8
−11.068	9.156	4.939	0.22429	HC-47	−2.270	7.203	10.126	0.19152	HC-9
−8.482	7.272	0.202	0.27118	HN	−1.106	6.539	5.796	0.20888	HC-12
−9.523	6.559	1.314	0.25517	HN	−0.338	5.235	6.764	0.21749	HC-12
−2.777	4.167	4.977	0.34902	HO-13	−1.921	4.947	5.965	0.22024	HC-12
−1.050	6.611	0.757	0.33563	HO-15	−2.248	7.271	7.873	0.20457	HC-11
−0.868	4.698	3.817	0.21594	HC-14	−0.230	6.652	21.179	0.38295	HO-1
−0.137	6.310	4.127	0.23222	HC-14	−3.382	9.147	23.939	−0.41985	C-34
−9.850	7.449	3.390	0.22701	HC-45	−1.969	8.665	24.396	−0.01814	C-35
−9.031	10.410	3.520	0.21726	HC-46	−2.160	7.890	25.573	−0.53953	O-35
−5.271	10.064	5.669	0.21808	HC-19	−1.261	7.875	23.362	−0.20620	C-36
−3.897	9.702	3.381	0.20841	HC-18	−1.928	6.758	22.716	−0.41110	C-37
−2.770	9.806	4.776	0.22875	HC-18	−1.907	5.491	23.440	−0.62546	C-38
−2.437	0.559	0.000	0.43866	HO-41P	0.166	7.374	23.939	−0.61099	C-39
−2.546	5.705	2.273	0.22436	HC-15	−3.857	10.230	24.941	−0.63371	C-40
−2.273	8.374	3.098	0.23622	HC-16	−2.634	8.422	26.262	0.33023	HO-35
−4.439	8.817	6.292	0.23685	HC-19	−1.406	5.632	24.409	0.22662	HC-38
−3.981	7.118	3.814	0.26547	HC-17	−2.938	5.147	23.606	0.20778	HC-38
−1.499	5.768	6.083	0.22252	HC-13	−1.360	4.741	22.849	0.20171	HC-38
−6.455	9.634	3.513	0.19888	HC-42	0.975	7.954	23.472	0.19645	HC-39
−8.105	9.019	1.589	0.21807	HC-44	0.193	7.520	25.029	0.21609	HC-39
−6.257	7.424	2.326	0.23720	HC-43	0.300	6.306	23.710	0.20698	HC-39
−1.189	6.569	21.420	−0.52265	O-1	−4.812	9.919	25.390	0.21146	HC-40
−1.909	6.255	20.346	0.51624	C-1	−3.102	10.355	25.731	0.19782	HC-40
−3.096	6.095	20.361	−0.43441	O-1	−3.995	11.184	24.411	0.21543	HC-40
−1.036	6.261	10.090	−0.48043	C-2	−3.315	9.568	22.925	0.20946	HC-34
−1.953	6.360	17.853	−0.01463	C-3	−1.333	9.538	24.602	0.20351	HC-35
−2.694	5.171	17.827	−0.52901	O-3	−2.970	7.074	22.561	0.20844	HC-37
−1.127	6.193	16.495	−0.38363	C-4	−4.111	8.324	23.916	0.21632	HC-34
−1.998	6.372	15.230	−0.01565	C-5	−0.979	8.534	22.527	0.20961	HC-36
−3.000	5.417	15.194	−0.52421	O-5	−1.434	6.631	21.741	0.20707	HC-37

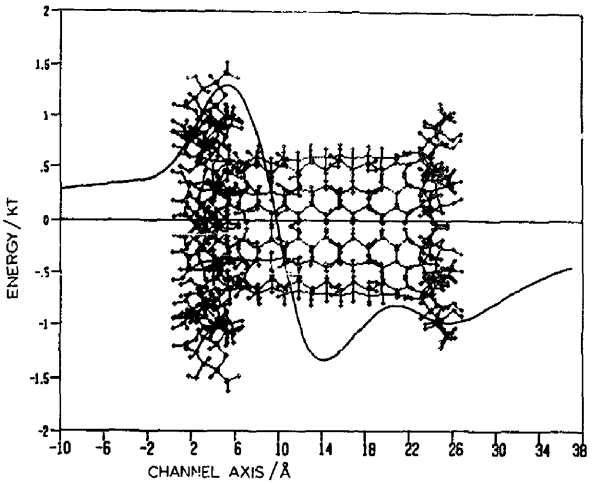

Fig. 6. Profile of the electrostatic potential energy for an octamer SLC with a radius of 4.47 Å. The pore starts at $Z = 0$ Å and ends at $Z = 26.3$ Å. The background figure represents this pore placed as described. The electrostatic energy (kT) and the Coulomb potential (V) have exactly the same pattern since there is only a Ze factor between them.

conduction than those obtained by previous theoretical models of a pore, (see for example Refs. 10–15).

We did not give too much weight to the numerical values of the interaction energies of the pores, because of the approximations made, what it is important is that all the structures considered have similar energies, with differences smaller than 12 kT, that correspond to a small portion of the total energies. This is the criterion that we used to make sure that within the frame of reference they are likely to occur.

Results

Electrostatic potential energy

Pores were built with the number of monomers, n, varying from 6 to 13 and R ranging from 4.47 to 7.2 Å.

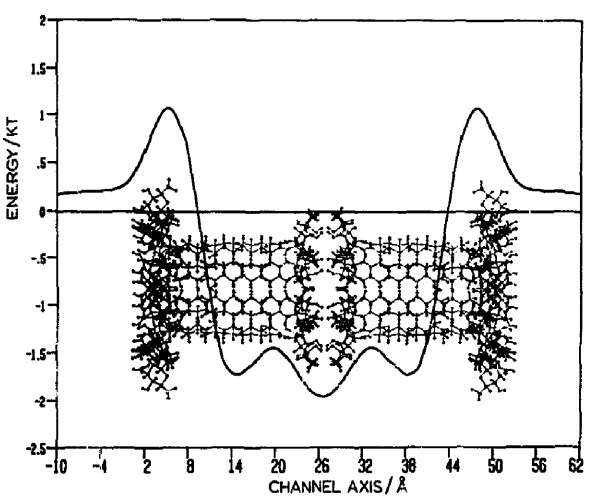

Fig. 7. Profile of the electrostatic potential energy for an octamer double-length channel with a radius of 4.47 Å. The pore starts at $Z = 0$ and ends at $Z = 52.6$ Å as shown in the background figure.

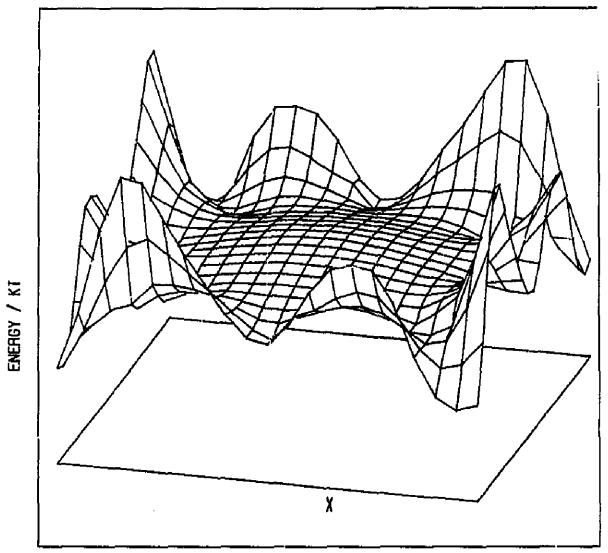

Fig. 8. The electrostatic potential surface at the plane X-Y and $Z = -1$ Å. This plane is reproduced in the figure (with a zero energy value) and the surface corresponds to the energy values at each point of the plane. The pore is an octamer with a radius of 4.47 Å.

Figs. 6 and 7 show the typical electrostatic potential energy profile of a cation moving through the pore axis of a single- and a double-length channel. (We would like to draw attention that one should not confuse the electrostatic energy potential with the transmembrane electric potential difference.) Figs. 8 and 9 present the surface potential of the energy near the pore mouth and the pore tail of an SLC. The purpose of these figures is

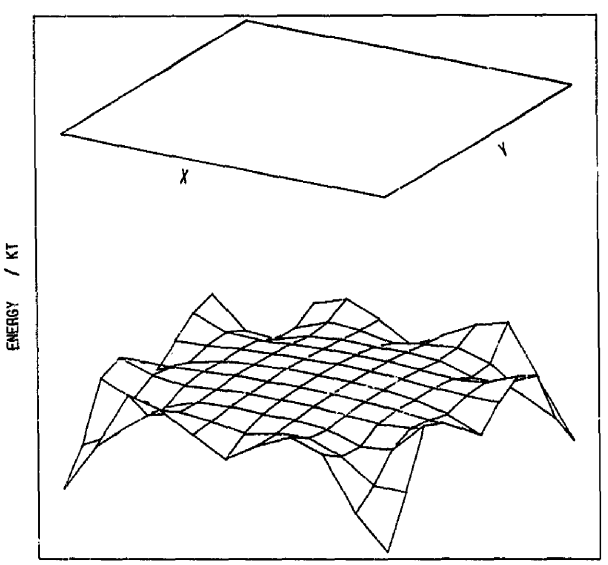

Fig. 9. The electrostatic potential surface at the plane X-Y and $Z = 27.5$ Å. This plane is reproduced in the figure (with a zero energy value) and the surface correspond to the energy values at each point of the plane. The limits of the plane are X and Y from -5 to 5. The pore is constructed from eight units and a radius of 4.47 Å.

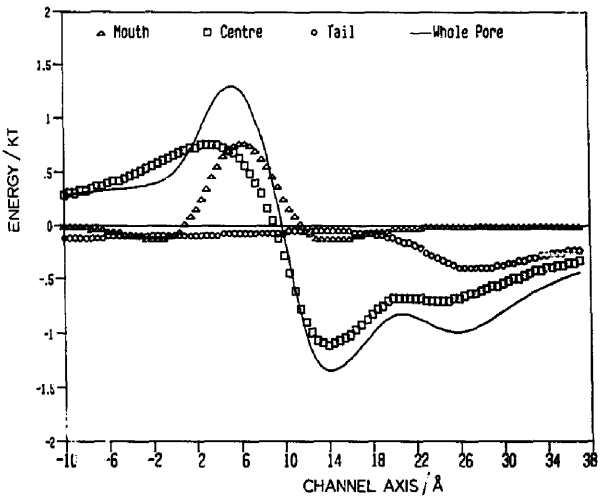

Fig. 10. Energy profile spectrum. Profiles of the electrostatic potential energy obtained for each of the three fragments of the pore considered (mouth, center and tail), and the resulting superposition. This corresponds to the octamer with a radius of 4.47 Å.

to show that the electrostatic potential energy behaves quite monotonically near the pore axis, i.e., there are no strong features in the vicinity of the center of the pore, supporting the idea of taking the central axis of the pore as the reaction path for the passage of ions.

Single length pore

(a) Energy profile spectrum. The electrostatic energy profiles corresponding to each of the three segments in which the whole molecule was divided appears in Fig. 10. The spectrum corresponds to the three fragments of an octamer channel with a radius of 4.47 Å. The structure is placed in such a way that the mouth extends from 0 to 6.3 Å, the center from 5.8 to 21.4 Å and the tail from 21.7 to 26.3 Å. The profile is due to a single positive charge moving along the axis of the pore.

The curve corresponding to the mouth shows a barrier (to cations) whose maximum is at about 6 Å. Far from the mouth this segment does not contribute appreciably; nevertheless, it causes, along with the center, the appearance of the only barrier of the profile. The energy profile due to the atoms of the center of the molecule presents a well (to cations) that vanishes smoothly from the center to the tail and in a steeper manner from the center to the mouth; the well minimum occurs at about 14 Å. The well shown in the whole channel profile is clearly due to this segment. It also must be noticed that near the mouth end the potential due to the center becomes positive and represents an important contribution to the whole profile. This means that the central region has a dipole pointing from the tail to the mouth and contributes, appreciably, to the cation barrier. Finally, even if the tail contribution seems to be less important compared to the other two segments, there is a small well, that added to the negative contribution of the central region, conforms an attractive zone for cations.

The main features of the whole channel profile are the well due to the central segment, the barrier due to the center and the mouth, and an extended depression due to the tail and the central segment. An overall description of an ion subject to this profile must be as follows: a cation feels attracted by the tail and repealed by the mouth. According to this scheme an SLC must be selective to cations approaching the pore by the tail region, as they find an attractive potential that begins at the tail neighborhood and extends up to the pore center. However, the cations approaching the channel from the mouth will find a barrier that extends quite away from it. For the anions the whole thing reverses. It is interesting to note that even if the electrostatic profiles near the tail and the mouth are different (those affecting selectivity) the heights of the barriers are very similar, rendering the electrostatic profile symmetric in spite of an obviously asymmetric structure. We would like to point out that this effect was obtained only when the contributions of the membrane was taken into account.

(b) Channels with the same radius and different molarity. The energy profiles of a set of channels with the same radius, $R = 4.47$ Å, and formed by 6 to 9 units are shown in Fig. 11. The general pattern of these energies exhibits a behavior that makes more pronounced the profile as the number of units increase. The fact that the potential increases with the number of monomers is a consequence of maintaining a constant radius and the additive approximation. What should be noted is that

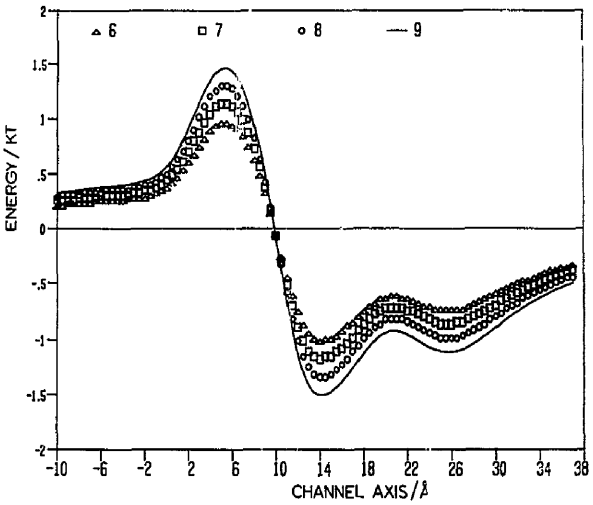

Fig. 11. Profile of the electrostatic potential energy for an SLC formed by 6, 7, 8 and 9 monomers keeping a constant radius of 4.47 Å. The pore starts at $Z = 0$ Å and ends at $Z = 26.3$ Å.

the increase from 6 to 9 units brings only a maximal increase in the energy of approx. 0.6 kT. With $R = 4.47$ Å it was rather difficult to construct pores with more than nine monomers, because of the repulsion that arises. It is quite simple to construct pores, as large as having 13 units, if one increases the radius up to 7 Å, but in this case, on the one hand, the model gives unstable structures (positive interaction energies) and, on the other hand, we can observe that the barrier at 4 Å tends to vanish, see Fig. 12. As will be discussed later, the fact would mean a loss of selectivity for the DLC.

(c) Channels with the same molarity and different radius. We have discussed so far the cases when the number of units that make up a pore vary while the radius is kept constant. What happens when the converse case occurs? Fig. 12 shows the results obtained for

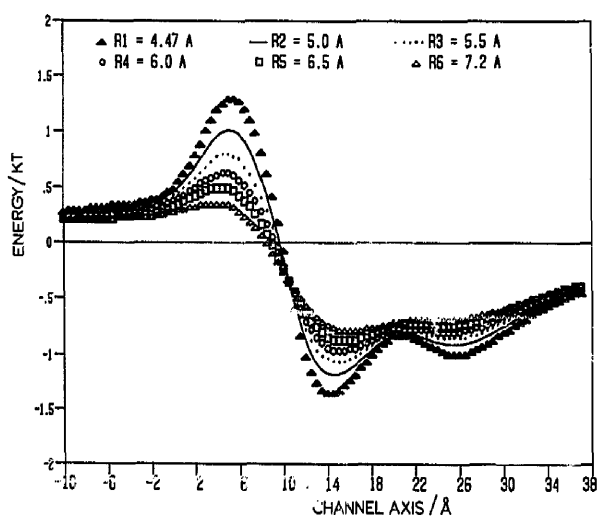

Fig. 12. Profiles of the electrostatic potential energy presented by octamers SLC formed by different radii, R_1 to R_6. Note that the profiles become less pronounced and the barriers at 4 Å and at 24 Å vanish, as the radius is increased.

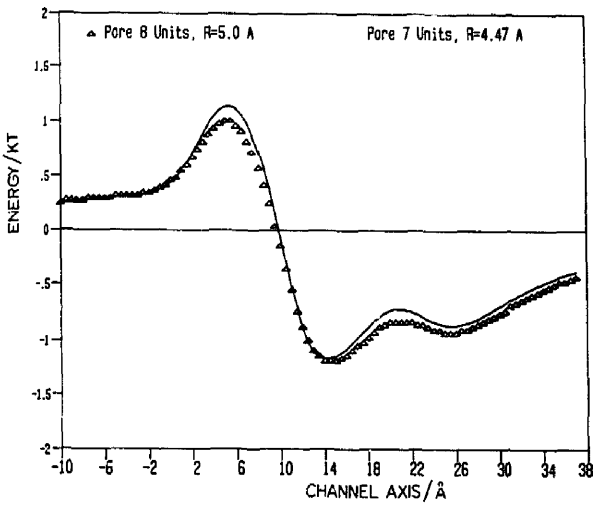

Fig. 13. Profiles of the electrostatic potential for two different pores, a heptamer with a radius $r = 4.47$ Å and an octamer with a radius $r = 5.0$ Å. Note the near equivalence of these profiles. This result reinforces the hypothesis of the existence of pores formed by different number of antibiotic molecules.

this case. The profiles follow the same general pattern as before and of course there appears an amplification due to a radius decrease. It should be noticed that barrier at 4 Å tends to disappear as the radius increases.

A cation coming near the tail of the smallest radius SLC will feel both a deep well and a high barrier, as the radius increases the depth of the well and the height of the barrier becomes less pronounced. Based on these profiles, one ought to make a compromise between the well deepness and the barrier height to choose the most efficient channel. Such election is made at the end, in terms of the pore radius and its units number. For instance, in Fig. 13 we can obtain practically the same electrostatic potential energy profile with an octamer of $R = 5$ Å and an heptamer of $R = 4.47$ Å.

Double length pore

A DLC is made up from two SLC. Based on the experiments of Kleinberg and Finkelstein [6], who tested the existence of single and double length channels of nystatin and amphotericin B, our model assumes that a double length channel is structurally two single length channels joined tail to tail. The proposed structure can be joined by hydrogen bonds that give more stability to the double length pore.

The DLC energy profile, Fig. 7, follows these assumptions: (i) the profile is symmetric to a plane perpendicular to the pore axis located at the tail end of the SLC. (ii) The DLC potential energy is obtained by superposition of the original SLC profile plus the symmetrically generated one. As a consequence of the DLC structure, the profile shows a pattern where the features corresponding to the SLC tails appear at the middle, while those of the mouths, at the extremes. Thus, it is easy to imagine the DLC profiles that will arise from the SLC we have presented. It should be noticed that the long-range cation attraction has vanished leaving only an anion attraction, with a substantial barrier for an anion in the central region.

The anion selectivity of this kind of channels is very likely determined by the wells at the pore entrances. Experimental single channels conductivities, for both SLC and DLC, are of 5 and 1 pS, respectively [6]. These values correspond to cations for the SLC and to anions for the DLC. For a cation passing through an SLC there is a barrier at 4 Å. For an anion passing through a DLC there is a broad barrier centered at approx. 26 Å. The anion barrier is about twice larger than the one for cations. As a result of this difference a cation finds easier to pass through an SLC than an anion through a DLC. It is interesting to note that our model can account, purely on electrostatic grounds, for this conductivity difference.

Discussion

With the results obtained, one can construct a microscopic image of the biological activity of the antibiotic, compare it with the known experimental observations and possibly make further predictions.

Here we propose that the SLC works by attracting cations through the tail end. A substantially smaller conductivity will be shown for the anions through the mouth end. The double length channel will be selective

to anions, since only mouths are facing the solution but with a reduced conductivity as compared to the single channel cations. For the above model to be true one has to allow for the possibility of the antibiotic appearing in a thin membrane with both orientations, even if added to only one side. Given the asymmetric character of the SLC, it seems to be quite necessary to have both orientations in order to have no rectification in the whole membrane measurements [6].

With the above model we can explain several experimental observations:

(a) Selectivity. The difference in the selectivity shown by the single and double length channels, unexplained until now, is due to the fact that in an SLC the tail of the pore is selective to cations, while in the DLC the mouth is selective to anions. There is also the observation [6] that the SLC selectivity is affected by changes in the ionic force, whereas the DLC selectivity is not. This can be explained through the difference between the two ion selective regions; in the SLC the cation well extends substantially into the bulk, see Fig. 6, whereas for the DLC the well to the anions is of a more local nature, see Fig. 7, and hence less exposed to changes in bulk concentration. We can also explain why divalent ions, either positive or negative are not translocated [6]. Of course, there are several factors to be considered, as the rigidity of the hydration shell in divalent ions, see for example Ref. 20, but from the simple fact of a two-fold increase in the potential profiles one can expect that the barriers would become unsurmountable.

(b) Conductance. It has been reported [23] that amphotericin B is a more effective translocator than nystatin for both, single and double length channels [6,23]. The only difference between the two antibiotics is that for amphotericin B an OH group is placed closer to the tail (by two C–C bonds) than in nystatin. This group is predicted to be negatively charged (net charge = $-0.1989\ e$) by molecular orbital calculation. If we imagine in Fig. 6, that this group, which is around 11 Å, gets moved to the left, thus simulating the profile for nystatin, we can see that both the cation-attraction of the tail and the anion-attractiveness of the mouth are reduced. We can also explain the lack of single channel rectification for the SLC, Ref. 6, which at first is surprising, as well as the relative size of the single channel conductance for the SLC (5 pS) and the DLC conductance (1 pS), Ref. 6.

It is interesting to note that for the whole membrane the above ratio is reversed, in spite that more monomers are needed for the construction of a DLC, the permeability of a double length channel is about 100-times larger, at the same antibiotic concentration [6]. This can be explained by the shorter opening times of the single channel for the SLC than for the DLC, see Ref. 6. This seems to suggest that the DLC has a more stable structure by the reduction of the wobbling of the tails.

There is also a surprising result in the permeabilities to nonelectrolytes. In spite of evidence that the DLC are of the same radii than the single length ones, the estimated conductance of glycerol and urea for a SLC is not just twice the double length conductance, but approx. 8-times, Ref. 6. Even if these two nonelectrolytes are neutral they have considerable dipole moments (i.e., urea 4.56 D), and certainly the passage through the electrostatic energy profile of a DLC is more difficult that through the SLC.

Finally, we can explain the general observation (Refs. 3–5,8) that the channels can present quite different molarities, but nonetheless quite similar permeabilities. We have seen in Fig. 13 how two channels of different molecularity present the same electrostatic profile of the passage of ions.

Conclusions

We have presented a microscopic model for an antibiotic channel based on first-principle calculations. We have seen that from the electrostatic potential energy obtained from the net charges, and their images on the membrane one is able to construct a model that explains the experimental observations, some of which had no explanation advanced up to now. The model is capable of presenting a microscopic image that predicts which molecular fragments are responsible for selectivity, conductivity and pore formation. Hence, chemical manipulation of this zone should conduce to variation of its conductance properties. The theoretical model is amenable of such improvement and since it is based on first principles and not on empirical parametrization this can be done in a stepwise manner. We are now computing the ion-antibiotic potential from the molecular orbital calculations themselves that would yield a more reliable estimation. Also the pore formation will be simulated through a Monte-Carlo study yielding the relative population of the different pores considered and a better exploration of the energy surface.

Acknowledgements

We would like to acknowledge one of the referees of this work for having suggested the manner in which to include the surrounding dielectric media of the pore. We would like also to thank J. Hernandez and R. Morales for technical assistance.

References

1 Laprade, R., Ciani, S.M., Eisenman, G. and Szabo, G. (1975) Membranes 3, 127–214.

2 McLaughlin, S. and Eisenberg, M. (1975) Annu. Rev. Biophys. Bioeng. 4, 335–365.
3 De Kruijff, B. and Demel, R.A. (1974) Biochim. Biophys. Acta 339, 57–70.
4 Cass, A., Finkelstein, A. and Krespi, V. (1970) J. Gen. Physiol. 56, 100–145.
5 Hoogevest, V.P. and De Kruijff, B. (1978) Biochim. Biophys. Acta 511, 397–407.
6 Kleinberg, M.E. and Finkelstein, A. (1984) J. Membr. Biol. 80, 257–269.
7 Andreoli, T.E. (1974) Ann. N.Y. Acad. Sci. 235, 469–479.
8 Ganis, P., Avitabile, G., Mechlinski, W. and Schaffner, C.P. (1971) J. Am. Chem. Soc. 93, 4560–4564.
9 Moreno-Bello, M., Bonilla-Marín, M. and González-Beltrán, C. (1988) Biochim. Biophys. Acta 844, 97–100.
10 Parsegian, A. (1969) Nature (London) 221, 844–846.
11 Levitt, D.G. (1978) Biophys. J. 22, 209–219.
12 Levitt, D.G. (1978) Biophys. J. 22, 221–248.
13 Jordan, P.C. (1980) Biophys. J. 39, 157–164.
14 Jordan, P.C. (1987) Biophys. J. 51, 297–311.
15 Sung, S.-S. and Jordan, P.C. (1987) Biophys. J. 51, 661–672.
16 Barthelat, J.C., Durand, Ph. and Serafini, A. (1971) Mol. Phys. 33, 181.
17 King, H.F. and Dupuis, M. (1976) J. Comp. Phys. 21, 144.
18 Les, A. and Ortega-Blake, I. (1987) Acta Phys. Pol. A72, 587–597.
19 Sierra, A. and Brickman, J. (1987) Biophys. J. 51, 969.
20 Ortega-Blake, I., Hernandez, J. and Novaro, O. (1984) J. Chem. Phys. 81, 1894–1900.
21 Clementi, E. (1985) J. Phys. Chem. 89, 4426.
22 Edmonds, d.T. (1985) Eur. Biophys. 13, 31.
23 Chen, W.C., Sud, I.J., Chou, D. and Feingold, D.S. (1977) Biochem. Biophys. Res. Commun. 74, 480–487.